TiO2 Nanocrystals Synthesized by Laser Pyrolysis for the Up-Scaling of Efficient Solid-State Dye-Sensitized Solar Cells

ARTICLE *in* ADVANCED ENERGY MATERIALS · OCTOBER 2011

Impact Factor: 16.15 · DOI: 10.1002/aenm.201100289

FULL PAPER

TiO_2 Nanocrystals Synthesized by Laser Pyrolysis for the Up-Scaling of Efficient Solid-State Dye-Sensitized Solar Cells

*Hussein Melhem, Pardis Simon, Layla Beouch, Fabrice Goubard, Mourad Boucharef, Catherine Di Bin, Yann Leconte, Bernard Ratier, Nathalie Herlin-Boime, and Johann Bouclé**

A crucial issue regarding emerging nanotechnologies remains the up-scaling of new functional nanostructured materials towards their implementation in high performance applications on a large scale. In this context, we demonstrate high efficiency solid-state dye-sensitized solar cells prepared from new porous TiO_2 photoanodes based on laser pyrolysis nanocrystals. This strategy exploits a reduced number of processing steps as well as non-toxic chemical compounds to demonstrate highly porous TiO_2 films. The possibility to easily tune the TiO_2 nanocrystal physical properties allows us to demonstrate all solid-state dye-sensitized devices based on a commercial benchmark materials (organic indoline dye and molecular hole transporter) presenting state-of-the-art performance comparable with reference devices based on a commercial TiO_2 paste. In particular, a drastic improvement in pore infiltration, which is found to balance a relatively lower surface area compared to the reference electrode, is evidenced using laser-synthesized nanocrystals resulting in an improved short-circuit current density under full sunlight. Transient photovoltage decay measurements suggest that charge recombination kinetics still limit device performance. However, the proposed strategy emphasizes the potentialities of the laser pyrolysis technique for up-scaling nanoporous TiO_2 electrodes for various applications, especially for solar energy conversion.

1. Introduction

Since the last decades, important advances in the field of nanotechnologies enabled major breakthroughs in various scientific domains, driven by the possibility of controlling and tuning the physical properties of materials at the nanoscale. In the current context of global warming and rising energy demand, these aspects are of particular importance, as new solutions arising from nanotechnologies already started to bring low-cost alternatives to existing issues. This is particularly true regarding solar energy conversion. Nanostructured organic or polymer solar cells demonstrated their strong potential as alternatives to expensive inorganic photovoltaic devices,[1,2] taking benefit from cheap processing routes such as printing techniques.[3] Alternatively, hybrid photo-electrochemical cells, or dye-sensitized solar cells (DSC),[4] demonstrate the highest power conversion efficiency to date among devices based on organic materials, with more than 12% for laboratory devices[5,6] and over 8% for submodules.[7,8] Although such performance requires a liquid electrolyte, they drove intensive efforts being made towards the up-scaling of cell fabrication on large areas using soft processing routes, in order to demonstrate low-cost and potentially flexible applications. Basically, the DSC consists of a porous titanium dioxide (TiO_2) film deposited on a transparent electrode and sensitized with a molecular monolayer of a light-absorbing dye.[9,10] This porous dye-sensitized electrode is then filled with a liquid electrolyte, and finally completed using a counter electrode. Following dye excitation under incident sunlight, ultrafast electron injection occurs in the TiO_2 conduction band, followed by electron transport through the metal oxide network to the collecting anode. In the meantime, dye regeneration is performed via oxydo-reduction reactions with the electrolyte (typically using the iodide/triiodide couple). Ultra-fast electron injection and dye regeneration ensure high production rate of free charge carriers in the metal oxide.[11] However, efficient photocurrent generation requires that electron transport in the percolating porous TiO_2 network, which is usually limited by trapping/detrapping mechanisms,[12,13] is significantly faster than charge recombination with the electrolyte. More recently, replacement of the

Mr. H. Melhem, Dr. M. Boucharef,[†] Dr. C. Di Bin,
Prof. B. Ratier, Dr. J. Bouclé
XLIM UMR 6172
Université de Limoges/CNRS
123 Avenue Albert Thomas
87060 Limoges Cedex, France
E-mail: johann.boucle@unilim.fr
Mrs. P. Simon, Dr. Y. Leconte, Dr. N. Herlin-Boime
IRAMIS/SPAM/LFP
CEA-CNRS URA 2453
Bât. 522, CEA Saclay
91191 Gif sur Yvette, France
Dr. L. Beouch, Prof. F. Goubard
Laboratoire de Physico-Chimie des Polymères et des Interfaces (LPPI)
Fédération Institut des Matériaux (FD 4122)
Université de Cergy-Pontoise
95031 Cergy-Pontoise Cedex, France
[†]Current affiliation: University Mentouri Constantine, Route Ein El Bey, 25017 Constantine, Algeria

DOI: 10.1002/aenm.201100289

liquid electrolyte by a quasi-solid[14–16] or solid-state[17,18] component was proposed to significantly reduce inherent leakages and improve device lifetimes, while reducing the number of the processing steps involved. In particular, all solid-state approaches using the molecular hole transporter 2,2′,7,7′-tetrakis-(N,N-di-p-methoxyphenylamine)-9,9′-spirobifluorene (spiro-OMeTAD) demonstrate over 6% efficiencies with significant stability, using both inorganic and organic dyes.[19–23] Due to a reduced number of processing steps, solid-state approaches present a true potential compared to liquid cells. Very recently, the first photovoltaic company was created in order to develop and commercialize the solid-state DSC technology (Oxford Photovoltaics Limited, Oxford, UK). However, efficient pore infiltration, which is a requirement to further improve device performance, remains difficult to achieve,[24,25] and a fine control of the porous layer morphology is required to assist the molecular glass penetration while reducing drastically charge recombination processes at the TiO_2-dye-spiroOMeTAD interface.

Despite the relatively high efficiencies of DSC among third generation solar cells, inexpensive and scalable processing steps are required for the demonstration of large area modules at low-cost. In this context, the porous TiO_2 photoanode is a critical component, which directly drives device performance. Conventional TiO_2 electrodes are deposited starting from nanocrystals synthesized either in solution using sol-gel procedure combined with hydrothermal growth, or by flame/furnace synthesis before being subsequently redispersed.[26–28] The obtained paste is compatible with various printing techniques, however, long steps at high pressures are required for the nanocrystal growth, and softer techniques are needed towards low cost manufacture of DSC modules. Aqueous synthesis has also been proposed to significantly reduce the requirement for cost-expensive growing steps,[29,30] but careful drying over several hours is still required in order to obtain TiO_2 nanocrystals with controlled physical properties.

In this context, we propose alternative porous TiO_2 electrodes processed from nanocrystals synthesized by laser pyrolysis. The method is based on the interaction in cross flow between a high power CO_2 laser beam and a gaseous or liquid precursor and has already demonstrated its versatility for the synthesis of various oxide and non-oxide NPs.[31,32] It requires no solvents and is intrinsically a clean process. Since 1987, The method has shown its efficiency for the production of TiO_2 nanocrystals presenting well-defined original properties from various titanium alkoxides such as titanium tetra-isopropoxide (TTIP).[33,34] The method is efficient for the production of TiO_2 nanocrystals presenting well-defined original properties.[35–37] The choice of experimental conditions allows controlling the flame temperature and TiO_2 in anatase or rutile phase with a controlled size from 8 to 25 nm with low size dispersion and a rutile to anatase ratio controlled in the range 5/95 to 95/5 could be obtained. Moreover, the technique allows the production at low cost of titania nanoparticles in a scalable way. Laser pyrolysis has already been scaled up for the production of silicon-based solar devices in the united states (Nanogram company) and will be further implanted in China under Nanogram licensing (2010). In France, a pilot plant scale compatible with high production rates ($kg.h^{-1}$) has been developed.[38] Finally, collection by direct dispersion of the obtained nanopowder in liquid phase is possible,[39] making laser pyrolysis a relevant technique for production up-scale.

In this paper, we describe the achievement of highly efficient solid-state dye-sensitized solar cells based on TiO_2 nanocrystals synthesized by laser pyrolysis, commercial organic dye, and solid-state electrolyte (spiro-OMeTAD). By a direct comparison with a TiO_2 porous electrode processed using a commercial TiO_2 paste (DYESOL), we evidence an efficient electrode infiltration by the molecular glass using laser pyrolysis nanocrystals, associated with state-of-the-art efficiencies. The results are discussed with regard to electrode morphology, as well as charge recombination probed by transient photovoltage decay measurements. These results demonstrate the relevance of laser pyrolysis for production up-scale of reproducible TiO_2 nanoparticles for photovoltaic energy conversion.

2. Results and Discussion

2.1. Properties of TiO_2 Nanocrystals Synthesized by Laser Pyrolysis

TiO_2 nanocrystals are synthesized using laser pyrolysis starting from titanium tetraisopropoxide (TTIP) as a liquid precursor,[36] using the Pyrosol process to generate an aerosol. The obtained nanopowders present well-defined morphology and structural properties that can be finely controlled by the main experimental parameters (flow of precursors, laser power density). Moreover, high production rates up to 20 $g.h^{-1}$ at the laboratory scale are evidenced using this process. In the present work, spherical nanoparticles are synthesized. The typical particle morphology, observed by transmission electron microscopy (TEM), is presented **Figure 1**a. The mean particle diameter is estimated to 12 nm from TEM images, with a narrow standard deviation in the order of 3 nm. The crystalline structure, evidenced by X-Ray Diffraction (Figure 1b), is compatible with a well-defined anatase TiO_2 phase, which is clearly dominant (>95%) with regard to rutile. The crystallite size is estimated from the diffraction peak full widths at half maximum using Scherrer's law to be around 11.6 nm diameter. The particles are found to be slightly agglomerated in the powder due to weak electrostatic interactions that are easily broken by sonication in various solvents, including water, as previously observed and reported in the literature for laser-synthesized nanoparticles.[39,40] In particular, the observation of a chain-like morphology is a specificity of laser-synthesized nanopowders.

2.2. Porous Electrode Fabrication and Solar Cell Performance

2.2.1. Paste Formulation and Deposition of Porous TiO_2 Electrodes

Electrode deposition requires the dispersion of the obtained nanocrystals in a solvent. The presence of polymeric additives or binders, such as poly(ethylene glycol) or ethyl-cellulose, is required in order to create a significant porosity in the films deposited from the suspension. The different concentrations in the paste drive the final viscosity, which has to be adapted to the deposition process to be used. Such procedures are well established concerning conventional liquid DSC,[26] and

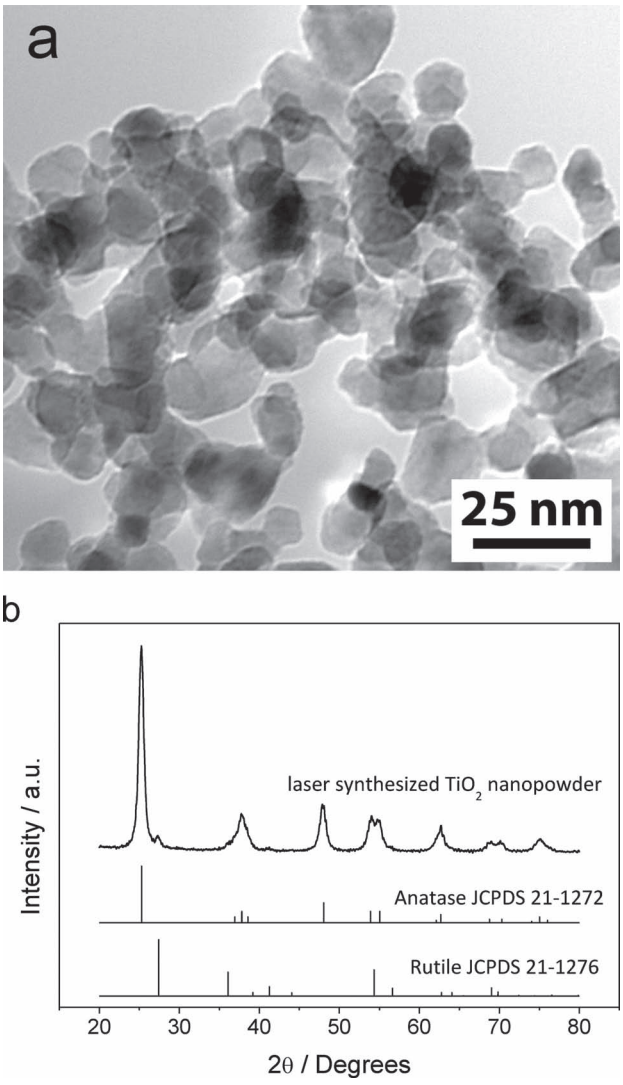

Figure 1. TEM image (a) and X-ray diffraction pattern (b) of the TiO_2 nanopowder synthesized by laser pyrolysis. The rutile and anatase contributions are represented in the diffraction pattern as well.

commercial pastes are now available from various specialized companies such as SOLARONIX S.A. (Switzerland), or DYESOL (Australia), where the typical TiO_2 content is usually in the range 15–20%wt.[26] For solid-state approaches, the use of a solid-state electrolyte such as the molecular glass spiro-OMeTAD, makes it difficult to entirely infiltrate a thick dye-sensitized TiO_2 electrode over several microns thick.[25] The use of highly absorbing dyes, presenting molar extinction coefficients over 50,000 M^{-1} cm^{-1} was found to be compatible with thinner porous electrodes,[21,41] and today's optimized solid-state DSC are obtained using 1.5 to 2.0 µm thick TiO_2 porous photoanodes.[42,43] Considering these thicknesses, several deposition techniques, such as screen-printing and spin-coating, are found suitable, and paste formulation was adapted to these particular approaches. In our case, a simple formulation procedure was used by dispersing 15%wt. of TiO_2 nanocrystals in ethanol, in the presence of ethyl-cellulose (TiO_2:ethyl-cellulose weight ratio of 3:2). After one hour of laboratory ultrasonic bath, the resulting paste is found suitable for film deposition using spin-coating, leading to 1.5 to 2 µm thick porous electrodes. A final sintering step using a temperature ramp up to 500 °C is finally used to remove the organic fraction and improve the TiO_2 particle interconnection and cristallinity, followed by $TiCl_4$ treatment (see experimental details). To assess the performance of the laser-synthesized TiO_2 nanocrystals, a reference TiO_2 electrode was deposited from a commercial TiO_2 paste purchased from DYESOL. **Figure 2** compares the morphology observed by SEM of the reference electrode with that of the electrode based on laser-synthesized TiO_2 nanocrystals. In general, the electrode morphology achieved using laser-synthesized nanocrystals is found to be very comparable to that obtained from sol-gel nanocrystals.[26,44–46] Only slight differences between the electrodes can be observed from these images. The mean pore diameter appears slightly smaller using the laser-synthesized nanocrystals. At the opposite, the amount of pores, or total pore volume, seems to appear larger for this electrode compared to the reference. Two factors can explain these observations: the intrinsically smaller dimension of the laser-synthesized nanocrystals (~ 12 nm) compared to the commercial paste (20 nm); the initial particle agglomeration in the paste. In particular, the particle aggregation in a chain-like

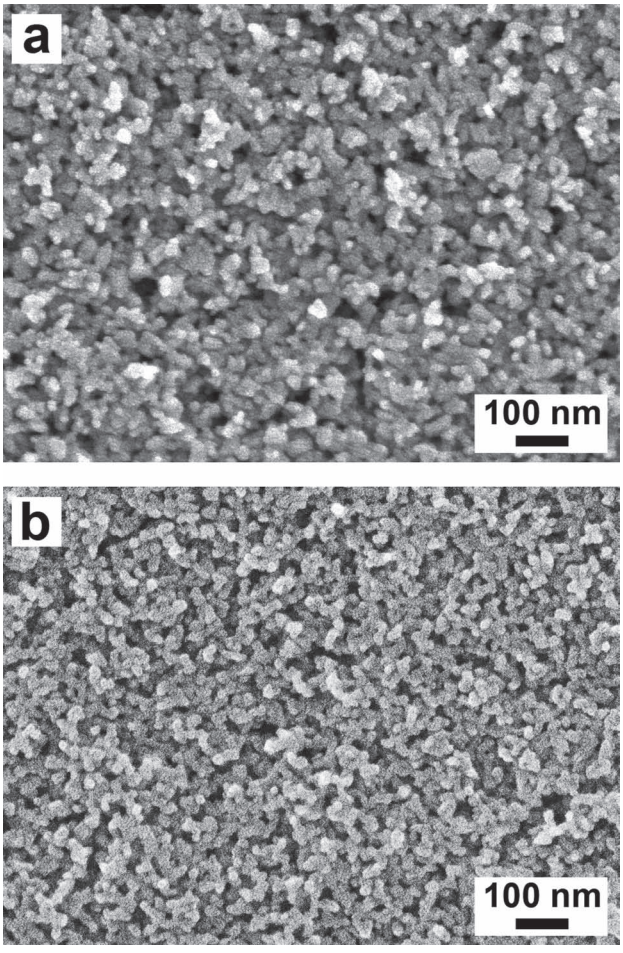

Figure 2. SEM images of the porous TiO_2 electrodes processed from the reference commercial paste (a) and from the formulation based on TiO_2 nanocrystals synthesized by laser pyrolysis (b).

morphology of laser-synthesized nanoparticles is likely to favor the achievement of nanostructured film of high porosity. We will discuss in the following sections the influence of electrode morphology on pore infiltration.

2.3. Performance of Solid-State DSC Based on Laser-Synthesized TiO_2 Electrodes

Solar cell fabrication is performed using conventional procedures,[47,48] starting from the porous TiO_2 photoanodes developed in this work deposited on fluorine tin oxide (FTO) substrates previously coated by spray pyrolysis by a thin TiO_2 compact layer, and commercial benchmark organic materials. The molecular glass 2,2′,7,7′-tetrakis(N,N-di-p-methoxypheny-amine)-9,9′-spirobifluorene (spiro-OMeTAD, Merck KGaA, Germany) is used as solid-sate electrolyte. The organic dye used in this work is the indoline derivative referred as D102 (Mitsubishi Paper Mills Limited, Japan), which demonstrate highly efficient solid-state devices with power conversion efficiencies up to 4.1%.[41] Although more efficient dyes have been reported since,[20–23] leading to efficiencies over 6% under 100 $mWcm^{-2}$, the D102 organic dye is commercially available, and does not require any co-adsorbents due to its non-planar geometry. This makes it a relevant benchmark material in the context of this study. Finally, the ruthenium-based N719 dye (Solaronix S.A.) is also used, as it constitutes a major reference material for liquid DSC, although power conversion efficiencies of solid-state DSC are limited to around 2% due to its low molar extinction coefficient.[49] The optical absorption spectra of devices based on reference TiO_2 and laser-synthesized TiO_2 electrodes, before the evaporation of gold top contact, are presented in **Figure 3**, for both N719 and D102 dyes. Very similar optical densities at the dye absorption maximum are evidenced between the reference device and the device based on laser-synthesized TiO_2. Using similar porous TiO_2 layer thicknesses, a much stronger fraction of light is however harvested in the case of D102 compared to N719, which is consistent with the higher molar extinction coefficient of the indoline dye (~ 55.10^3 M^{-1} cm^{-1}) compared to the ruthenium dye (~ 14.10^3 M^{-1} cm^{-1}).[41] Considering that the laser-synthesized electrode is slightly thicker than the reference electrode, the similar optical densities observed for both electrodes sensitized with D102 could indicate a slight difference in electrode morphology. This aspect will be discussed in the following sections. The performance of the corresponding devices, measured under simulated solar emission (AM1.5G, 100 mW cm^{-2}) are given **Figure 4**a, while **Table 1** summarizes the associated photovoltaic parameters. It is worth noting that the reported

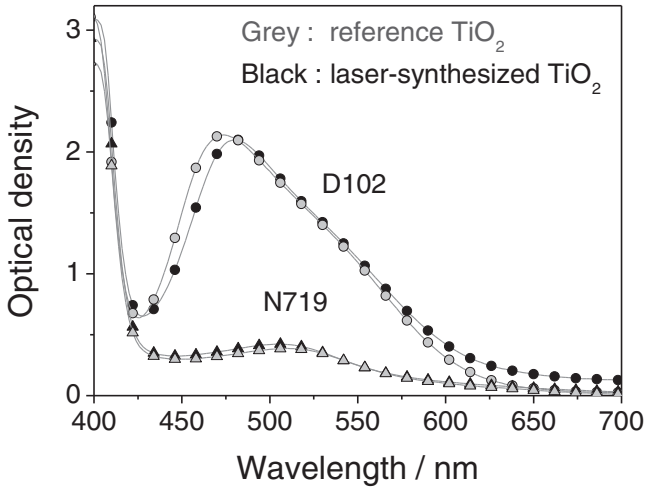

Figure 3. Optical absorption spectra of solid-state DSC based on porous TiO_2 electrodes processed from the reference paste (grey symbols) and the paste based on laser-synthesized nanocrystals (black symbols). The spectra, given for both N719 (triangles) and D102 (circles) dyes, correspond to a solar cell structure FTO/dense TiO_2/porous TiO_2/dye/spiro-OMeTAD. Reference TiO_2 layers are 1.75 μm thick, and laser-synthesized TiO_2 are 1.85 μm thick.

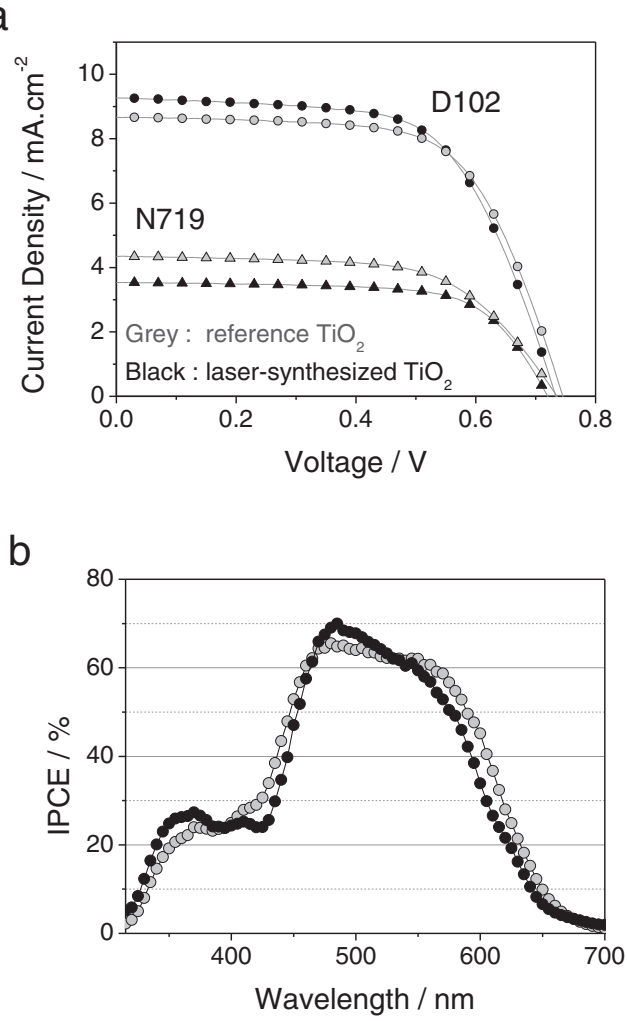

Figure 4. Current-voltage characteristics (a) of solid-state DSC devices based on reference TiO_2 electrode (grey symbols) and electrode based on laser-synthesized TiO_2 nanocrystals (black symbols), for both N719 (triangles) and D102 (circles) dyes. Measurements are performed under 100 $mW.cm^{-2}$, AM1.5G simulated solar spectrum. The IPCE spectra (b) of devices based on D102 are also presented (b) for the reference TiO_2 electrode (grey symbols) and the electrode based on laser-synthesized nanocrystals (black symbols).

Table 1. Photovoltaic parameters under simulated solar emission (100 mW.cm^{-2}, AM1.5G) of the different devices investigated in this work as a function or TiO_2 electrode type and dye: short-circuit current density (J_{SC}); open-circuit voltage (V_{OC}); fill factor (FF); power conversion efficiency (η).

Cell type	Dye	J_{SC} [mA.cm^{-2}]	V_{OC} [mV]	FF	η [%]
Reference	N719	4.34	740	0.61	1.97
Laser-synthesized TiO_2	N719	3.53	720	0.67	1.76
Reference	D102	8.66	750	0.64	4.13
Laser-synthesized TiO_2	D102	9.27	740	0.61	4.23

Table 2. Thicknesses of porous TiO_2 and spiro-OMeTAD overlayer, as well as weight fraction of spiro-OMeTAD infiltrated in the TiO_2 pores (X) and filling fraction for prous TiO_2/D102 structures based on reference and laser-synthesized TiO_2 pastes.

Electrode type	Porous TiO_2 thickness [µm]	Thickness of spiro-OMeTAD overlayer [nm]	X [%]	Filling Fraction [%]
Reference TiO_2	1.85	150	21	58
Laser-synthesized TiO_2	1.75	25	26	77

photovoltaic parameters correspond to individual solar cells. The corresponding performance are representative of several sets of measurements performed on different set of cells. Devices based on the high molar extinction coefficient dye (D102) are associated with the highest photocurrent generation, as expected. For both dyes, the laser-pyrolysis TiO_2 electrode presents an overall power conversion efficiency comparable with that of the electrode processed from the commercial paste. This result demonstrates that laser pyrolysis is a relevant technique for the production of TiO_2 nanocrystals compatible with an efficient photovoltaic energy conversion. The achievement of a 4.23% efficient cell with D102 is mainly associated with an increased short-circuit current density (J_{SC}) compared to the reference device. This aspect will be discussed in the following sections by considering the possible influence of the electrode specific area and its ability for pore filling. The incident photon to current efficiency (IPCE) spectra of devices based on D102 are presented Figure 4b. Comparable contributions to current generation are evidenced for both devices, except that the IPCE is found to be slightly improved in the low wavelength region below 400 nm using laser-synthesized TiO_2 nanocrystals. However, the IPCE spectrum is found narrower than that of the reference device, as well as that of previously reported solid-state DSC,[23] suggesting that device operation is not optimal. This effect could be a direct consequence of the TiO_2 surface states, which are likely to be dependent on the particle used for electrode processing. We will describe this particular aspect in the following sections.

2.4. Influence of Electrode Morphology on Pore Filling and Device Operation

2.4.1. Pore Filling versus Electrode Morphology

DSC operation results from several factors. The porous TiO_2 photoanode is a crucial component which has various influences on charge generation, recombination and current collection. The key factors that have to be considered are the crystalline structure of TiO_2, the electrode morphology (porosity, pore dimensions and specific surface area), and the nature of surface states. In the following section, we will focus on the electrode morphology and its influence of pore filling by the molecular hole transporter, as well as on the influence of trap sites and surface states on the charge dynamics at the interface. Considering the different starting particle diameters, SEM observations (see Figure 2) reveals a comparable electrode morphology when using laser-synthesized nanocrystals compared to the reference TiO_2 paste, although more quantitative investigations would be required to evaluate the exact porosity and pore distribution. An estimation of the relative surface area developed by the laser-synthesized electrode is obtained through a comparison of the optical absorption of D102-sensitized electrodes with regard to non-sensitized electrodes. Considering that no noticeable aggregation on TiO_2 is observed using D102, a measure of the relative absorbance of the dye for both the laser-synthesized and reference electrodes allows us to evaluate the specific area of the laser-synthesized electrode relatively to the reference (Supporting Information, Figure S1 and Table S2). In particular, it appears that for similar film thicknesses, the laser-synthesized electrode is grafted with around 22% less dye molecules than the reference electrode processed from the commercial paste. This observation is compatible with a lower surface area of the laser-synthesized electrodes. This is also consistent with the optical absorption of the cells reported in Figure 3, as a thicker laser-synthesized electrode was required to harvest as much photons as the reference device.

2.5. Pore Filling versus Electrode Morphology

Solid-state DSC operation is known to be strongly sensitive to the fraction of solid electrolyte that fills the dye-sensitized TiO_2 electrode pores. In particular, poor TiO_2-dye/spiro-OMeTAD interfaces are responsible for rapid charge recombination, leading to poor current generation. Proper device operation requires an intimate contact of the TiO_2-dye with the hole transporter medium in order to ensure efficient hole transfer and hopping to the gold anode. In this context, pore filling is a crucial parameter, that can be estimated using different techniques such as SEM cross-sections,[50] energy dispersive X-ray spectroscopy (SEM-EDX),[51] or X-ray photoelectron spectroscopy (XPS) depth profiling.[25] While the first technique is only qualitative, the two latter methods can be tricky to implement for routine analyses. Simple empirical calculations of pore filling have also been reported,[24] based on the understanding of the processes that occurs during the deposition of spiro-OMeTAD by spin-coating. In general, the filling fraction, which is defined as the ratio between the volume of infiltrated spiro-OMeTAD and the volume of the pores, is estimated to be in the order of 60-65%, up to 85% for the more optimistic estimations. A major mechanism that ensures efficient infiltration is capillarity. In that context, pore dimensions and electrode morphology are important parameters, which have been found to govern hole transporter infiltration more critically, rather that the nature of the dye

for example. In this work, we use a simple method to determine the filling fraction of dye-sensitized TiO_2 electrodes by organic hole transporters, based on the measurement of the weight losses of infiltrated electrodes by differential thermogravimetric analysis (TGA).[52] The filling fraction can be easily expressed as:

$$Filling\ Fraction\ = \frac{X \times d_{Tio_2}(1-\phi)}{\phi \times d_{spiro}(100-X)} \times 100 \quad (1)$$

Where X is the weight fraction of spiro-OMeTAD infiltrated in the TiO_2 pores with regard to the total weight of TiO_2 and spiro-OMeTAD infiltrated. φ is the porosity of the TiO_2 electrode. $d_{TiO2} = 4$ g cm^{-3} and $d_{spiro} = 1.82$ g cm^{-3} are the densities of the TiO_2 and spiro-OMeTAD respectively.[25] The weight fraction X of infiltrated spiro-OMeTAD can be deduced from TGA measurements performed on 10 cm^2 dye-sensitized TiO_2 substrates, with and without spiro-OMeTAD. This estimation requires the exact knowledge of the spiro-OMeTAD overlayer thickness that remains after deposition by spin-coating, as well as of the porous electrode thickness. These thicknesses are accurately measured from SEM cross-sections as depicted **Figure 5** for infiltrated devices based on D102. Surprisingly, the thickness of the spiro-OMeTAD overlayer is found to be very different between both electrodes, with only 25 nm for the laser-synthesized electrodes compared to 150 nm for the reference device, despite the fact that similar parameters have been used for the deposition of spiro-OMeTAD by spin-coating. This observation suggests that a larger amount of molecular glass infiltrates the laser-synthesized electrode compared to the reference. **Figure 6** presents the TGA analysis up to 600 °C under synthetic air of D102-sensitized electrodes, with and without spiro-OMeTAD. Several processes occurs as temperature increases. An initial weight loss of 2% occurs around 40 °C for bare and infiltrated sensitized electrodes, due to moisture desorption. Then, weight losses associated with the thermal degradation of the molecular glass (for infiltrated electrodes), and of the D102 dye are observed. By comparing the TGA curves of bare and infiltrated TiO_2 porous electrode, the weight fraction of spiro-OMeTAD inside the TiO_2 pores can be deduced. From these measurements, an estimation of the filling fraction can be made, assuming a relative electrode porosity φ of 50% for both systems. This value includes the porosity shrinkage due to dye infiltration, as reported in the literature for reference TiO_2 electrodes.[25,53] More quantitative porosity measurements are now being considered, however, we assume that a porosity of 50% is an upper limit for the porosity of the dye-coated laser-synthesized electrode, based on SEM observations and UV-visible absorption spectroscopy performed on dye-sensitized electrodes. Therefore, and considering equation (1), the filling fraction extracted for the laser-synthesized TiO_2 electrode is likely to be a lower estimate. The different device layer thicknesses and porous electrode filling fractions are summarized Table 1. A reasonable pore filling of 60% is achieved with the reference TiO_2 electrode, which is consistent with reported values.[25] However, significant improvements are demonstrated using the porous TiO_2 electrode based on laser-synthesized nanocrystals, where the filling fraction reaches 80%. This improvement is likely to be a consequence of the different electrode morphologies. Especially, a smaller pore diameter resulting from the use of particles with smaller diameters favors capillarity forces, which are crucial in the infiltration process. Both SEM and TGA analyses are consistent with an improved pore infiltration by spiro-OMeTAD when using laser-synthesized nanocrystals. The specific electrostatic agglomeration of as-formed laser-synthesized nanopowders, which results in a chain-like morphology, is a crucial parameter in this context. This result is consistent with the collection of a larger current density for this electrode.

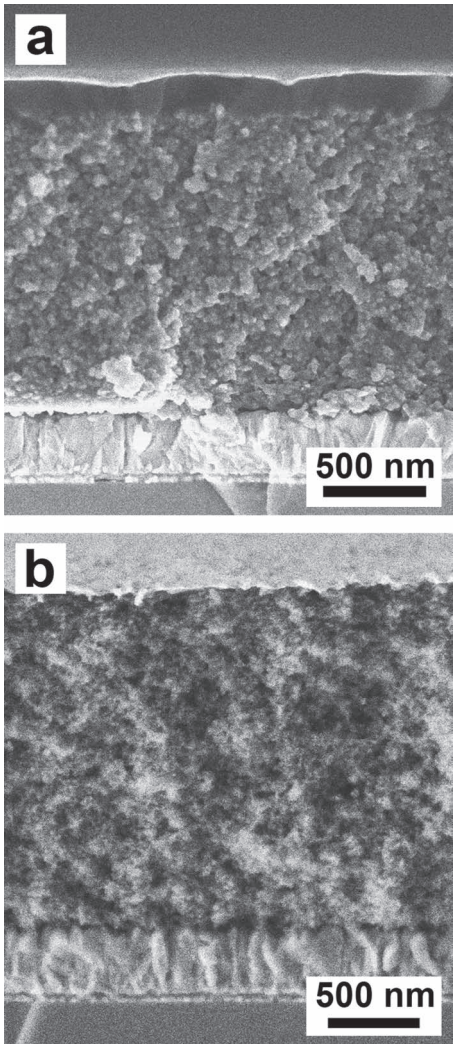

Figure 5. SEM cross sections of full devices (FTO/dense TiO_2/porous TiO_2/D102/spiro-OMeTAD/Au) made from porous TiO_2 electrodes processed from reference commercial TiO_2 paste (a) and paste made from laser-synthesized TiO_2 nanocrystals (b).

2.5.1. Charge Kinetics Probed by Transient Photovoltage

Device performance emphasize a significant improvement of J_{SC} when using the laser-synthesized nanocrystals compared to the reference TiO_2. Our analysis indicates that a slightly lower specific area of the electrode compared to the reference is compensated by an improved pore filling. However, a slight

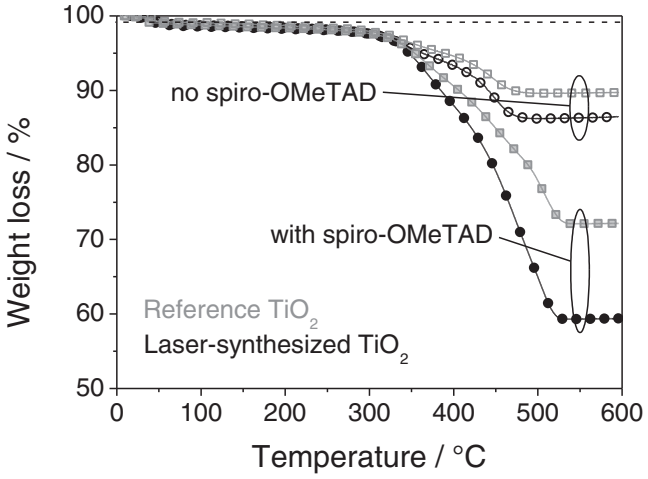

Figure 6. Weight losses measured by TGA of D102-sensitized TiO_2 electrodes based on laser-synthesized nanocrystals without (grey triangles) and with (black triangles) infiltration of spiro-OMeTAD.

decrease in the open-circuit voltage (V_{OC}) is observed. Several physical parameters can influence V_{OC}, such as charge recombination at the dye/spiro-OMeTAD interface, TiO_2 band edge shift, or trap distribution associated with TiO_2 surface states. Transient photovoltage decay measurement is a simple characterization technique from which charge recombination kinetics can be extracted.[54] In open-circuit conditions, no charge can flow in the external circuit so that the photovoltage decay is associated with charge recombination only. Under low perturbation regime, the photovoltage decay can be fitted using a mono-exponential function, from which a pseudo-recombination rate constant (k) can be extracted. **Figure 7**a shows the recombination rate constants measured by transient photovoltage of solid-state DSC devices based on reference and laser-synthesized TiO_2 electrodes. A larger recombination rate constant is evidenced for the laser-synthesized TiO_2 electrode compared to the reference. This observation is consistent with faster charge recombination events at the TiO_2/dye/spiro-OMeTAD interface, which result in the slightly lower V_{OC} measured for this cell compare to the reference. Moreover, slightly different slopes in the $k = f(J_{SC})$ curves are evidenced between both devices. Considering that the dependence of J_{SC} on incident light power density is found to be linear in both cases, as depicted Figure 7b, this observation reveals the strong influence of trap density on charge kinetics. Especially, the trap distribution in TiO_2 is found to be dependent on the paste used. Several reports emphasized the strong influence of the textural and structural properties of the TiO_2 surface on device operation.[46,55] Especially, the surface structure of the titania colloid significantly influences the photovoltaic parameters of the cells. It was also shown that the nature of post-treatments used after electrode deposition is an important parameter that controls the interfacial properties and energetics of TiO_2,[56] illustrating the strong sensitivity of the electrode to the process used. Surface states, which can act as trap sites for electron, have direct influences on both charge transport and recombination.[12,55] In our case, further investigations will be required in order to get a detailed overview of the physical processes that drives the

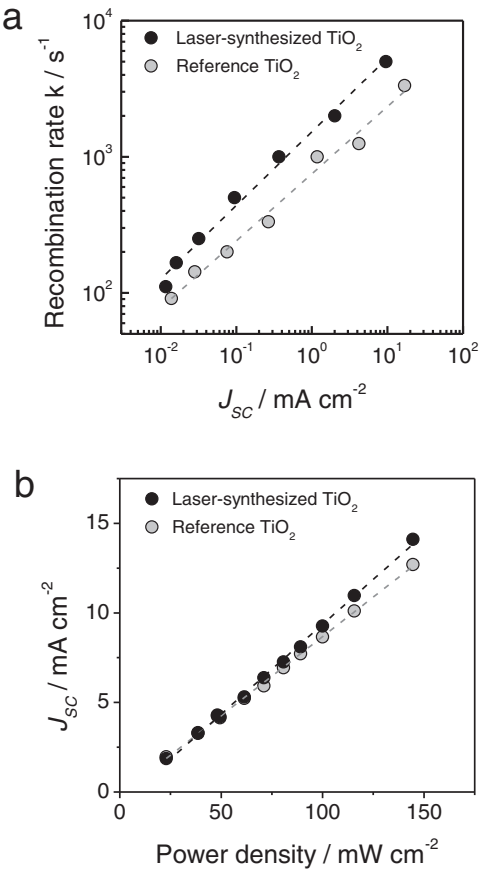

Figure 7. Charge recombination rates (a) of devices based on the reference TiO_2 electrode (grey circles) and the electrode based on laser-synthesized TiO_2 nanocrystals (black circles). The recombination rate constants (k) are extracted from transient photovoltage measurements performed at open-circuit under various light intensities. The bottom axis shows the corresponding short-circuit current density J_{SC}, measured under similar light intensities in short-circuit conditions. The dependence of J_{SC} on incident light intensity is also presented (b) for the same devices.

charge kinetics under operation conditions as a function of the main parameters involved. Nevertheless, a higher trap density is expected using TiO_2 nanocrystals of small diameters, which is consistent with the observations made by transient photovoltage on laser-synthesized nanocrystals (mean diameter of 12 nm) in comparison with the reference system (particles with a mean diameter of 20 nm). Such trend was observed by Zhu and coworkers by varying the porosity of TiO_2 photoanodes using nanocrystals of various diameters.[57] In particular, they showed that charge recombination mainly occurs via surface states rather than from the TiO_2 conduction band. In our case, further experiments are being performed to decouple the influence of surface states, as well as of film morphology, on charge kinetics and device performance.

3. Conclusion

In conclusion, we demonstrate for the first time highly efficient solid-state DSC based on TiO_2 porous electrodes processed

from laser-synthesized nanocrystals. The corresponding power conversion efficiency under full sunlight are comparable with that of state-of-the-art reference devices based on commercial TiO_2, mainly due to an improved current generation. Despite a lower specific area compared to the reference, pore infiltration by the molecular glass spiro-OMeTAD is found to be significantly improved using laser-synthesized nanocrystals with estimated filling fraction up to 80% compared to 60% for the reference electrode. This behavior is thought to be favored by using particles with smaller diameter, and by the natural tendency of laser-synthesized nanopowders to cluster in a chain-like morphology. Although charge recombination is found to be slightly faster using laser-synthesized TiO_2 nanoparticles, leading to reduced open-circuit voltages, the possibility to finely tune the nanocrystal properties during the synthesis allows further potential improvements, using doping for example. Considering the compatibility of laser pyrolysis for production up-scale, these results suggest that the technique is relevant for the synthesis of nanocrystals presenting reproducible physical properties, well-adapted for photovoltaic applications.

4. Experimental Section

Synthesis of TiO2 nanocrystals by laser pyrolysis: Titanium dioxide nanopowders were prepared by the laser pyrolysis method,[31,36] using titanium tetraisopropoxide (TTIP) as a liquid precursor. This technique is based on the resonance between the emission of a CO_2 laser (10.6 µm) and the absorption of a gaseous or liquid precursor. Briefly, an aerosol of TTIP (Sigma–Aldrich, used as received) was produced by an ultrasonic spraying technique (Pyrosol process) and carried to the reaction chamber by a carrier gas flow (Argon) where it intersected orthogonally the CO_2 laser beam. A sensitizer gas, C_2H_4, was also added because of its resonant absorption at the CO_2 laser radiation. The reactor pressure was fixed to 740 Torr, and the laser power was fixed at 1 kW. The obtained nanoparticles were then carried by the Argon flow to filters where they were collected. After the synthesis, the obtained powders contained free carbon coming from TTIP and C_2H_4 decomposition. In order to remove these carbon phases, the sample was submitted to soft thermal treatment in air at 400 °C during 3 hours.

Paste formulation and fabrication of solid-state DSCs: the TiO_2 nanocrystals are dispersed in ethanol (10 wt.%, around 90 mg ml^{-1}) before a suitable amount of ethyl-cellulose (EC), previously dissolved in ethanol, is added in the formulation to reach a TiO_2:EC weight ratio of 3:2. The resulting TiO_2 paste is placed in an ultrasonic bath for 1h and finally spin-coated on a fluorinated tin oxide substrate (FTO, 10 Ω/£) in air to obtain 1.5 to 2.0 µm thick TiO_2 films. The FTO substrate is previously cleaned and covered with a 250 nm thick TiO_2 dense layer deposited by chemical spray pyrolysis.[58] For the reference devices, the porous electrode is processed by spin-coating starting from a commercial TiO_2 paste (DSL 18NRT, Dyesol) previously diluted at 50% by ethanol. The porous TiO_2 electrodes are sintered following a temperature rampage up to 500 °C over 45 min on a hotplate in air. A conventional $TiCl_4$ treatment is then performed,[47,59] and the films are immersed for 15h at 80 °C in a diluted solution (0.3 mM in ethanol) of either RuL2(NCS)2:2TBA (L = 2,2′-bipyridyl-4,4′-dicarboxylic acid; TBA = tetrabutylammonium, N719, Solaronix S.A.), or indoline dye (D102, Mitsubishi Paper Mills), both used as received. The dye-sensitized TiO_2 electrodes are then rinsed and infiltrated by the molecular hole conductor 2,2′,7,7′-tetrakis(N,N-dip-methoxypheny-amine)-9,9′-spirobifluorene (spiro-MeOTAD, Merck KGaA) from spin-coating, using conventional procedures, except that no chemical p-dopant was used ($SbCl_4$). Gold top electrodes were finally evaporated under vacuum (10^{-6} mbar) using shadow masks that define two active areas per substrates (0.18 cm^2 each).

Evaluation of pore filling: Preparation of samples was carried out on glass subsrates (4 cm^2) and was identical to that of photovoltaic devices. The powder is recovered by scraping. Thickness and microscopy measurements on glass support were systematically performed to check that all powder has been extracted for analyze. Thermogravimetric analysis (TGA) were realized in air with a TA Instrument Q50 at a heating rate of 20 °C mn^{-1}.

Characterization techniques: Transmission electron microscopy (TEM) images (Philips CM12, using a W cathode, operated at 120 kV) of the laser pyrolysis TiO_2 nanocrystals were recorded by dispensing a few microliters of a diluted suspension in ethanol onto carbon-coated copper observation grids X-Ray diffraction (XRD) patterns were obtained with a Philips D500 diffractometer operating with Cu Kα radiation. Crystallite sizes were evaluated using (101) anatase peak and the Scherer formula. Scanning electron microscopy (SEM) was performed using a JEOL MEBFEG 7400F on porous TiO_2 layers and complete solar cell cross-sections, which were cut prior to the analysis. Current density-voltage (J-V) characteristics were recorded in air using a Keithley 2400 source-measure unit, in the dark and under simulated solar emission (Atlas Solarconstant 575PV). The spectral mismatch between the emission of the solar simulator and the global AM1.5G solar spectrum (ASTM G173-03) was corrected using a mismatch factor[60] and the solar simulator irradiance was adjusted accordingly using a certified silicon reference cell in order to achieve an equivalent AM1.5G irradiance of one sun (100 mW cm^{-2}) on the test cells. The incident photon to current efficiency (IPCE) was estimated using a monochromated 75W xenon lamp (Newport). The photocurrent, measured in static regime by a calibrated pico-amperemeter (Keithley 485), was compared to the calibration current measured with a calibrated silicon photodetector of known spectral response (Newport). Transient photovoltage decay measurements were performed on complete working solar cells in order to probe the charge kinetics under open-circuit conditions, using a technical setup described elsewhere.[48,61] The incident white illumination, provided by OSRAM LEDs, varied up to approximately 100 mW cm^{-2} on the devices, in order to probe the intrinsic charge kinetics under realistic working conditions. For each light intensities, the short-circuit current density of the devices was measured, before an additional light pulse, provided by a LED controlled by a solid-state switch, was applied under open-circuit conditions in order to extract the decay time $\tau = 1/k$ from a mono-exponential function.

Supporting Information

Supporting Information is available from the Wiley Online Library or from the author.

Acknowledgements

J. B. gratefully acknowledges the "Région Limousin" and the University of Limoges for a "Contrat Renforcé Recherche" (C2R–2007/2009), as well as the "Programme pluridisciplinaire Energie" of the CNRS (COLHYBRDIE project–2010/2011). J. B. thanks Dr. Henry J. Snaith for useful discussions concerning various aspects on the processing and characterization of solid-state DSCs. Mr. Pierre Carles is acknowledged for SEM observations on porous electrodes and devices.

Received: May 30, 2011
Published online: August 4, 2011

[1] S. Günes, H. Neugebauer, N. S. Sariciftci. *Chem. Rev.* **2007**, *107*, 1324.
[2] V. Shrotriya. *Nature Photonics* **2009**, *3*, 447.
[3] F. C. Krebs. *Sol. Energy Mater. Sol. Cells* **2009**, *93*, 1636.
[4] B. O'Regan, M. Grätzel. *Nature* **1991**, *353*, 737.

[5] Y. Chiba, A. Islam, Y. Watanabe, R. Komiya, N. Koide, L. Han. *Japanese Journal of Applied Physics, Part 2: Letters* **2006**, *45*, L638.
[6] F. Gao, Y. Wang, D. Shi, J. Zhang, M. Wang, X. Jing, R. Humphry-Baker, P. Wang, S. M. Zakeeruddin, M. Grätzel. *J. Am. Chem. Soc.* **2008**, *130*, 10720.
[7] L. Han, A. Fukui, Y. Chiba, A. Islam, R. Komiya, N. Fuke, N. Koide, R. Yamanaka, M. Shimizu. *Appl. Phys. Lett.* **2009**, *94*.
[8] H. Arakawa, T. Yamaguchi, T. Sutou, Y. Koishi, N. Tobe, D. Matsumoto, T. Nagai. *Current Applied Physics* **2010**, *10*, S157.
[9] M. Grätzel. *Journal of Photochemistry and Photobiology C: Photochemistry Reviews* **2003**, *4*, 145.
[10] A. Hagfeldt, G. Boschloo, L. Sun, L. Kloo, H. Pettersson. *Chem. Rev.* **2010**, *110*, 6595.
[11] Y. Tachibana, J. E. Moser, M. Grätzel, D. R. Klug, J. R. Durrant. *J. Phys. Chem.* **1996**, *100*, 20056.
[12] A. J. Frank, N. Kopidakis, J. V. D. Lagemaat. *Coord. Chem. Rev.* **2004**, *248*, 1165.
[13] L. Peter. *Acc. Chem. Res.* **2009**, *42*, 1839.
[14] S. M. Zakeeruddin, M. Grätzel. *Adv. Funct. Mater.* **2009**, *19*, 2187.
[15] B. Li, L. Wang, B. Kang, P. Wang, Y. Qiu. *Sol. Energy Mater. Sol. Cells* **2006**, *90*, 549.
[16] Y. Wang. *Sol. Energy Mater. Sol. Cells* **2009**, *93*, 1167.
[17] H. J. Snaith, L. Schmidt-Mende. *Adv. Mater.* **2007**, *19*, 3187.
[18] J. H. Yum, P. Chen, M. Grätzel, M. K. Nazeeruddin. *ChemSusChem* **2008**, *1*, 699.
[19] U. Bach, D. Lupo, P. Comte, J. E. Moser, F. Weissörtel, J. Salbeck, H. Spreitzer, M. Grätzel. *Nature* **1998**, *395*, 583.
[20] M. Wang, J. Liu, N.-L. Cevey-Ha, S.-J. Moon, P. Liska, R. Humphry-Baker, J.-E. Moser, C. Grätzel, P. Wang, S. M. Zakeeruddin, M. Grätzel. *Nano Today* **2010**, *5*, 169.
[21] M. Wang, M. Xu, D. Shi, R. Li, F. Gao, G. Zhang, Z. Yi, R. Humphry-Baker, P. Wang, S. M. Zakeeruddin, M. Grätzel. *Adv. Mater.* **2008**, *20*, 4460.
[22] M. Wang, S. J. Moon, M. Xu, K. Chittibabu, P. Wang, N. L. Cevey-Ha, R. Humphry-Baker, S. M. Zakeeruddin, M. Grätzel. *Small* **2010**, *6*, 319.
[23] N. Cai, S.-J. Moon, L. Cevey-Ha, T. Moehl, R. Humphry-Baker, P. Wang, S. M. Zakeeruddin, M. Graätzel. *Nano Lett.* **2011**, *11*, 1452.
[24] H. J. Snaith, R. Humphry-Baker, P. Chen, I. Cesar, S. M. Zakeeruddin, M. Grätzel. *Nanotechnology* **2008**, *19*.
[25] I. K. Ding, N. Tétreault, J. Brillet, B. E. Hardin, E. H. Smith, S. J. Rosenthal, F. Sauvage, M. Grätzel, M. D. McGehee. *Adv. Funct. Mater.* **2009**, *19*, 2431.
[26] S. Ito, T. N. Murakami, P. Comte, P. Liska, C. Grätzel, M. K. Nazeeruddin, M. Grätzel. *Thin Solid Films* **2008**, *516*, 4613.
[27] K. E. Lee, C. Charbonneau, G. Shan, G. P. Demopoulos, R. Gauvin. *JOM* **2009**, *61*, 52.
[28] S. E. Pratsinis, W. Zhu, S. Vemury. *Powder Technol.* **1996**, *86*, 87.
[29] Y. Li, Y. Fan, Y. Chen. *J. Mater. Chem.* **2002**, *12*, 1387.
[30] R. Chu, J. Yan, S. Lian, Y. Wang, F. Yan, D. Chen. *Solid State Commun.* **2004**, *130*, 789.
[31] W. R. Cannon, S. C. Danforth, J. H. Flint, J. S. Haggerty, R. A. Marra. *J. Am. Ceram. Soc.* **1982**, *65*, 324.
[32] M. Cauchetier, O. Croix, M. Luce. *Advanced Ceramic Materials* **1988**, *3*, 548.
[33] J. D. Casey, J. S. Haggerty. *Journal of Materials Science* **1987**, *22*, 4307.
[34] M. Grujić-Brojčin, M. J. Šćepanović, Z. D. Dohčević-Mitrović, I. Hinić, B. Matović, G. Stanišić, Z. V. Popović. *J. Phys. D: Appl. Phys.* **2005**, *38*, 1415.
[35] H. Maskrot, N. Herlin-Boime, Y. Leconte, K. Jursikova, C. Reynaud, J. Vicens. *J. Nanopart. Res.* **2006**, *8*, 351.
[36] B. Pignon, H. Maskrot, V. G. Ferreol, Y. Leconte, S. Coste, M. Gervais, T. Pouget, C. Reynaud, J. F. Tranchant, N. Herlin-Boime. *Eur. J. Inorg. Chem.* **2008**, 883.
[37] P. Simon, B. Pignon, B. Miao, S. Coste-Leconte, Y. Leconte, S. Marguet, P. Jegou, B. Bouchet-Fabre, C. Reynaud, N. Herlin-Boime. *Chem. Mater.* **2010**, *22*, 3704.
[38] A. Reau, B. Guizard, C. Mengeot, L. Boulanger, F. Ténégal. *Mater. Sci. Forum* **2007**, *534–536*, 85.
[39] C. Sentein, B. Guizard, S. Giraud, C. Yé, F. Ténégal. *J. Phys.: Conference Series* **2009**, *170*.
[40] J. Bouclé, N. Herlin-Boime, A. Kassiba. *J. Nanopart. Res.* **2005**, *7*, 275.
[41] L. Schmidt-Mende, U. Bach, R. Humphry-Baker, T. Horiuchi, H. Miura, S. Ito, S. Uchida, M. Grätzel. *Adv. Mater.* **2005**, *17*, 813.
[42] M. Wang, C. Grätzel, S.-J. Moon, R. Humphry-Baker, N. Rossier-Iten, S. M. Zakeeruddin, M. Grätzel. *Adv. Funct. Mater.* **2009**, *19*, 2163.
[43] H. J. Snaith, A. Petrozza, S. Ito, H. Miura, M. Grätzel. *Adv. Funct. Mater.* **2009**, *19*, 1810.
[44] C. J. Barbé, F. Arendse, P. Comte, M. Jirousek, F. Lenzmann, V. Shklover, M. Grätzel. *J. Am. Ceram. Soc.* **1997**, *80*, 3157.
[45] Z. Tebby, O. Babot, D. Michau, L. Hirsch, L. Carlos, T. Toupance. *Journal of Photochemistry and Photobiology A: Chemistry* **2009**, *205*, 70.
[46] A. Zaban, S. T. Aruna, S. Tirosh, B. A. Gregg, Y. Mastai. *The Journal of Physical Chemistry B* **2000**, *104*, 4130.
[47] H. J. Snaith, L. Schmidt-Mende, M. Grätzel, M. Chiesa. *Physical Review B - Condensed Matter and Materials Physics* **2006**, *74*.
[48] M. Boucharef, C. Di Bin, M. S. Boumaza, M. Colas, H. J. Snaith, B. Ratier, J. Bouclé. *Nanotechnology* **2010**, *21*.
[49] J. Krüger, R. Plass, M. Grätzel, H. J. Matthieu. *Appl. Phys. Lett.* **2002**, *81*, 367.
[50] L. Schmidt-Mende, M. Grätzel. *Thin Solid Films* **2006**, *500*, 296.
[51] A. J. Moulé, H. J. Snaith, M. Kaiser, H. Klesper, D. M. Huang, M. Grätzel, K. Meerholz. *J. Appl. Phys.* **2009**, *106*.
[52] J. Dehaudt, L. Beouch, S. Peralta, C. Plesse, P. H. Aubert, C. Chevrot, F. Goubard. *Thin Solid Films* **2011**, *519*, 1876.
[53] C. J. Barbé, F. Arendse, P. Comte, M. Jirousek, F. Lenzmann, V. Shklover, M. Grätzel. *J. Am. Ceram. Soc.* **1997**, *80*, 3157.
[54] B. C. O'Regan, F. Lenzmann. *J. Phys. Chem. B* **2004**, *108*, 4342.
[55] J. van de Lagemaat, A. J. Frank. *The Journal of Physical Chemistry B* **2000**, *104*, 4292.
[56] Z. Tebby, O. Babot, T. Toupance, D. H. Park, G. Campet, M. H. Delville. *Chem. Mater.* **2008**, *20*, 7260.
[57] K. Zhu, N. Kopidakis, N. R. Neale, J. Van De Lagemaat, A. J. Frank. *J. Phys. Chem. B* **2006**, *110*, 25174.
[58] L. Kavan, M. Grätzel. *Electrochim. Acta* **1995**, *40*, 643.
[59] L. Vesce, R. Riccitelli, G. Soscia, T. M. Brown, A. Di Carlo, A. Reale. *J. Non-Cryst. Solids* **2010**, *356*, 1958.
[60] J. M. Kroon, M. M. Wienk, W. J. H. Verhees, J. C. Hummelen. *Thin Solid Films* **2002**, *403–404*, 223.
[61] R. Radbeh, E. Parbaile, J. Bouclé, C. Di Bin, A. Moliton, V. Coudert, F. Rossignol, B. Ratier. *Nanotechnology* **2010**, *21*.

ADVANCED ENERGY MATERIALS

Supporting Information

for *Adv. Energy Mater.*, DOI: 10.1002/aenm.201100289

TiO_2 Nanocrystals Synthesized by Laser Pyrolysis for the Up-Scaling of Efficient Solid-State Dye-Sensitized Solar Cells

*Hussein Melhem , Pardis Simon , Layla Beouch , Fabrice Goubard , Mourad Boucharef , Catherine Di Bin , Yann Leconte , Bernard Ratier , Nathalie Herlin-Boime , and Johann Bouclé **

Submitted to ADVANCED ENERGY MATERIALS

Supporting Information

for *Adv. Energy Mater.*, DOI: 10.1002/aenm.201100289

TiO_2 nanocrystals synthesized by Laser Pyrolysis for the Up-Scaling of Efficient Solid-State Dye-Sensitized Solar Cells

Hussein Melhem, Pardis Simon, Layla Beouch, Fabrice Goubard, Mourad Boucharef, Catherine Di Bin, Yann Leconte, Bernard Ratier, Nathalie Herlin-Boime, and *Johann Bouclé**

Influence of porous TiO_2 electrode morphology on dye loading

Here, we compare the optical absorption properties of TiO_2 porous electrodes based on laser-synthesized nanocrystals compared with the reference electrode prepared from a commercial TiO_2 paste. The net optical absorption of the dye is compared in both cases (Figure S1), starting from 1.9 μm thick porous electrodes, and after subtracting the contribution of the FTO/dense TiO_2/porous TiO_2 electrode. The ratio between the integral of the absorbance curves gives an estimate of the relative specific area between both electrodes (see Table S2).

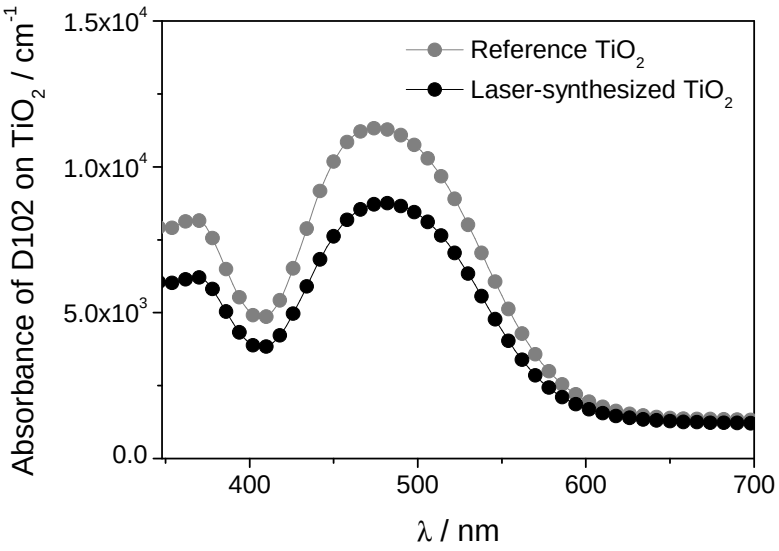

Figure S1. Contribution of the D102 dye to the optical absorbance of 1.9 μm thick dye-sensitized porous TiO_2 electrodes prepared from laser-synthesized TiO_2 nanocrystals (black

circles) compared with the reference electrode prepared from the commercial TiO_2 paste (DYESOL). The contribution of the substrate (glass/FTO/dense TiO_2/porous TiO_2) was subtracted in each case.

Table S2. Estimate of the relative specific area of the laser-synthesized TiO_2 electrode with regard to the reference electrode for a given electrode thickness, obtained from the ratio between the integrals of the absorbance curves of Figure S1.

Porous electrode	Relative surface area [%]
Reference TiO_2	100
Laser-synthesized TiO_2	78